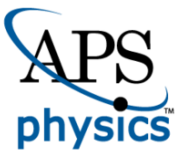

Effect of gravity on capillary instability of liquid jets

Ghobad Amini, Matthias Ihme, and Ali Dolatabadi

Phys. Rev. E **87**, 053017 — Published 22 May 2013

DOI: 10.1103/PhysRevE.87.053017

Effect of Gravity on Capillary Instability of Liquid Jets

Ghobad Amini[a,1], Matthias Ihme[b], and Ali Dolatabadi[c]

a Department of Aerospace Engineering, University of Michigan, Ann Arbor, MI 48109

b Department of Mechanical Engineering, Stanford University, Stanford, CA 94305

c Department of Mechanical and Industrial Engineering, Concordia University, Montreal, QC, Canada, H3G1M8

ABSTRACT

The effect of gravity on the onset and growth rate of capillary instabilities in viscous liquid jets is studied. To this end, a spatial linear stability analysis of Cosserat's equations is performed using a multiscale expansion technique. A dispersion relation and expressions for the perturbation amplitude are derived to evaluate the growth rate of the most-unstable axisymmetric disturbance mode. Modeling results are compared with classical results in the limit of zero Bond number, confirming the validity of this approach. Expressions for the critical Weber number, demarcating the transition between convective and absolute instability are derived as function of capillary and Bond numbers. Parametric investigations for a range of relevant operating conditions (characterized by Capillary, Weber, and Bond numbers) are performed to examine the jet break-up and the perturbation growth-rate. In addition to the physical insight that is obtained from this investigation, the results that are presented in this work could also be of relevance as test-cases for the algorithmic development and the verification of high-fidelity multiphase simulation codes.

[1] E-mail: aminibaz@umich.edu

I. INTRODUCTION

Instability and breakup of liquid jets is important for a wide range of applications, including liquid fuel injection, coating, drug delivery, food preparation, and ink-jet printing [1]. By neglecting surrounding gas-effects and gravity, Rayleigh [2] demonstrated that the origin of the jet breakup is the hydrodynamic instability. He showed that a circular cylindrical liquid jet is unstable with respect to disturbances of wavelengths larger than the jet circumference. Keller et al. [3] argued that unstable disturbances grow over space as they are convected along the downstream direction. Leib & Goldstein [4, 5] studied the absolute instability of liquid jets, arising from a saddle-point singularity in the dispersion relation. In contrast to the convective instability analysis of Keller et al. [3], the disturbances in an absolutely unstable liquid jet propagate in both upstream and downstream directions.

Although gravitational effects have been considered in the past for specific applications [1], the effect of gravity on capillary instabilities of low-speed liquid jets has not been investigated. Reasons for this are the complexity of breakup processes and the extension of the parametric manifold, requiring the consideration of the coupling between inertia, viscous forces, surface tension, and gravity.

In the Rayleigh breakup regime, which is relevant for low-speed jets, surrounding gas effects are negligible and the breakup mechanism is due to capillary pinching. Depending on the relative magnitude of gravitational, inertia, viscous, and surface tension forces, gravity could affect the instability dynamics. Therefore, providing a fundamental physical understanding about gravitational effects on the primary jet break-up has the potential to better control breakup length and drop-size [1, 6, 7].

Developing an analytic model for describing the onset of capillary instabilities of free-surface flows from three-dimensional detailed conservation equations introduces unnecessary complexities. Therefore, consideration of a set of simplified equations that captures the essential physics in the linear stability regime enables the development of a tractable analytical method to obtain fundamental insight. Green [8] developed such a formulation and derived a one-dimensional model for a straight, circular, viscous jet using the basic theory of the one-dimensional Cosserat's continuum equations. Cosserat's equations can be systematically derived from the Navier-Stokes equations through a Taylor-series expansion [9] or through an averaging method over the cross-sectional plane using Galerkin projection techniques [10]. The resulting governing equations are high-order nonlinear partial differential equations [1]. This 1-D model, inherently containing radial inertia effects, describes the jet profile, velocity, and pressure as function of the axial coordinate only, and simplifies the analysis considerably. Bogy [11-14] used Cosserat's equations successfully to study the stability of circular liquid jets in linear and nonlinear regimes. More recently, Amini & Dolatabadi [15, 16] analyzed the temporal and spatial stability of viscous elliptic jets using Cosserat's theory in the absence of gravitational forces.

The objective of this work is to investigate the Rayleigh instability of viscous liquid jets under consideration of gravitational forcing along the jet direction. To this end, a multiscale expansion of the one-dimensional Cosserat's equations is performed, and the mean flow is obtained from the numerical solution of the steady-state Cosserat's equations. The governing equations and linearized form are presented in the next section. From the linearized Cosserat's equations, an analytic dispersion relation is derived. Using this relation, the instability dynamics is parametrically investigated in Sec. IV. The paper finishes with conclusions.

II. GOVERNING EQUATIONS

The present analysis considers the instability of a liquid jet in the presence of inertia, viscosity, capillary, and gravitational forces. The problem configuration that is considered in the present work and relevant parameters are schematically illustrated in Fig. 1.

The complete set of Cosserat's equations includes conservation equations for mass and momentum, which after eliminating pressure among axial and radial momentum equations [17], can be written in non-dimensional form as

$$\left(r^2\right)_t + \left(r^2 v\right)_z = 0, \tag{1a}$$

$$\begin{aligned} & r^2(v_t + v v_z) - \frac{1}{2} r^3 r_z \left(v_{zt} + v v_z - \frac{1}{2} v_z^2 \right) - \frac{1}{8} r^4 (v_{zzt} + v v_{zzz}) = \\ & \frac{1}{\mathrm{We}} \left[\left(\frac{r}{(1+r_z^2)^{1/2}} + \frac{r^2 r_{zz}}{(1+r_z^2)^{3/2}} \right)_z + \mathrm{Ca} \left(3 r^2 v_z - \frac{1}{8} (r^4 v_{zz})_z \right)_z + \mathrm{Bo}\, r^2 \right] \end{aligned} \tag{1b}$$

where r is the liquid jet-radius and v is the velocity component in axial direction (see Fig. 1). These variables are functions of axial distance, z, and time, t. Subscripts z and t represent partial derivatives with respect to axial distance and time, respectively. The interested reader is referred to Ref. [10], which provides a detailed derivation of Eqs. (1). Equation (1b) describes the balance between momentum, on the left, and capillary, viscosity, and gravitational forces, on the right. All quantities in Eqs. (1) are non-dimensionalized by using the initial jet radius R^* and the axial jet exit velocity V^* as

$$r = \frac{r^*}{R^*}, \qquad v = \frac{v^*}{V^*}, \qquad z = \frac{z^*}{R^*}, \qquad t = \frac{t^* V^*}{R^*}, \tag{2}$$

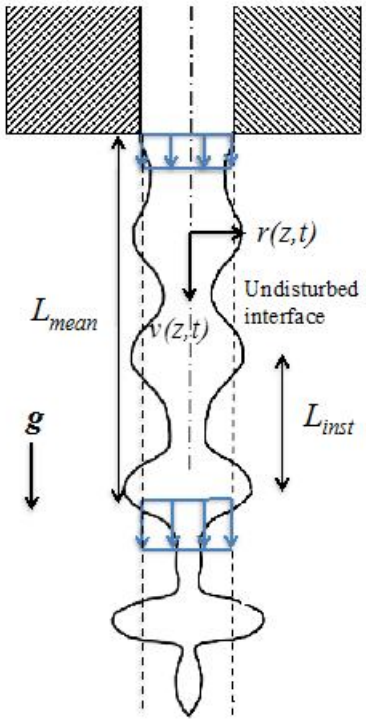

FIG. 1. (Color online) Schematic of liquid jet and relevant quantities.

and an asterisk refers to a dimensional quantity. Through this non-dimensionalization, the following dimensionless groups can be identified:

Weber number: $$\mathrm{We} = \frac{\rho^* V^{*2} R^*}{\sigma^*} \tag{3a}$$

Reynolds number: $$\mathrm{Re} = \frac{\rho^* V^* R^*}{\mu^*} \tag{3b}$$

Froude number: $$\mathrm{Fr} = \frac{V^{*2}}{g^* R^*} \tag{3c}$$

Capillary number: $$\mathrm{Ca} = \frac{\mu^* V^*}{\sigma^*} = \frac{\mathrm{We}}{\mathrm{Re}} \tag{3d}$$

Bond number: $$\mathrm{Bo} = \frac{\rho^* R^{*2} g^*}{\sigma^*} = \frac{\mathrm{We}}{\mathrm{Fr}} \tag{3e}$$

In these equations, μ^* is the dynamic viscosity, ρ^* is the density, σ^* is the surface tension, and g^* is the gravitational acceleration.

In the following, effects of Bond number and other controlling parameters on the instability dynamics of liquid jets are investigated by employing a multiscale stability analysis.

III. MULTISCALE STABILITY ANALYSIS

For a local linear stability analysis, the state-variables in Eqs. (1) are decomposed into a mean and a fluctuating quantity, viz.,

$$r(t,z) = \bar{r}(z) + r'(t,z) \tag{4a}$$

$$v(t,z) = \bar{v}(z) + v'(t,z). \tag{4b}$$

In the following analysis, the base-flow quantities $\bar{r}$ and $\bar{v}$ are obtained from the numerical solution of the steady-state form of Cosserat's equations (1), which can be written as:

$$\left(\bar{r}^2 \bar{v}\right)_z = 0, \tag{5a}$$

$$\bar{r}^2 \bar{v}\bar{v}_z - \frac{1}{2}\bar{r}^3 \bar{r}_z \left(\bar{v}\bar{v}_{zz} - \frac{1}{2}\bar{v}_z^2\right) - \frac{1}{8}\bar{r}^4 \bar{v}\bar{v}_{zzz} = \frac{1}{\mathrm{We}}\left[\left(\frac{\bar{r}}{(1+\bar{r}_z^2)^{1/2}} + \frac{\bar{r}^2 \bar{r}_{zz}}{(1+\bar{r}_z^2)^{3/2}}\right)_z + \mathrm{Ca}\left(3\bar{r}^2 \bar{v}_z - \frac{1}{8}(\bar{r}^4 \bar{v}_{zz})_z\right)_z + \mathrm{Bo}\,\bar{r}^2\right]. \tag{5b}$$

The numerical scheme for the solution of these nonlinear coupled equations employs a staggered formulation. An upwind-biased scheme is used to approximate all convective terms and all other operators are discretized by central differencing schemes. Inflow conditions are enforced by

Dirichlet conditions, and convective outflow conditions are used at the exit of the computational domain. The discretized equations are solved implicitly using an iterative scheme.

The spatio-temporal evolution of the hydrodynamic instabilities is described using a multiscale analysis technique [18, 19]. The underlying assumption of this analysis is that the base flow varies slowly in the axial direction compared to the perturbed flow. To consider this scale-disparity, a slowly varying coordinate, X, is introduced

$$X = \varepsilon z, \tag{6}$$

and ε is defined as

$$\varepsilon = \frac{L_{inst}}{L_{mean}}, \tag{7}$$

comparing the characteristic scales of the instability L_{inst} to the characteristic length of the mean-flow deformation L_{mean} (see Fig. 1). In the present analysis, L_{inst} is associated with the perturbation wavelength and L_{mean} is defined as

$$L_{mean} = \min\left(\frac{\bar{v}}{d\bar{v} / dz} \right). \tag{8}$$

To assess the validity of the perturbation analysis, ε is evaluated from Eq. (7) over the range of operating conditions that are considered in this work. From the results, presented in Fig. 2, it can be seen that ε remains less than 0.1 for $Bo \leq 1$, therefore justifying a weakly non-parallel mean flow approximation.

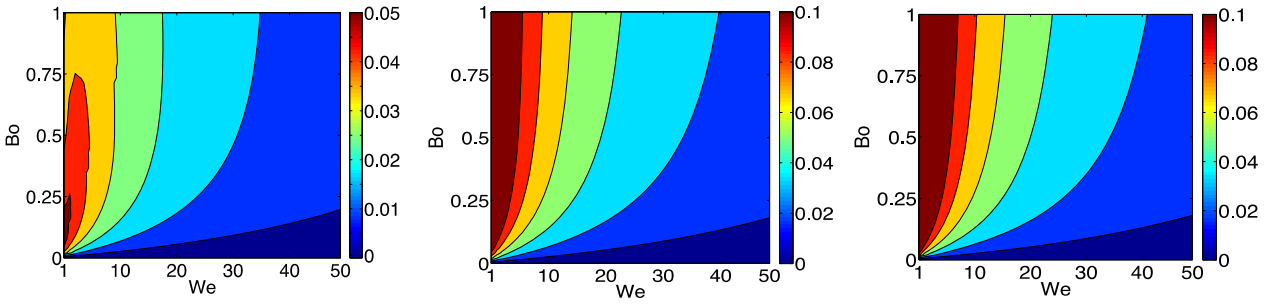

(a) Re = 0.1 (b) Re = 10 (c) Re = 1000

FIG. 2. (Color online) Variation of non-parallel flow indicator, ε, as function of We and Bo numbers for different Reynolds numbers: (a) Re = 0.1, (b) Re = 10, and (c) Re = 1000.

Toward the spatial stability analysis of Eqs. (1), the perturbed radius and axial velocity are represented by normal modes of the form

$$r' = [\hat{r}_0(X) + \varepsilon \hat{r}_1(X)] \exp\left\{ i \left(\frac{1}{\varepsilon} \int^X \alpha(X) dX - \omega t \right) \right\}, \tag{9a}$$

$$v' = [\hat{v}_0(X) + \varepsilon \hat{v}_1(X)] \exp\left\{ i \left(\frac{1}{\varepsilon} \int^X \alpha(X) dX - \omega t \right) \right\}, \tag{9b}$$

where $\hat{r}_0(X)$, $\hat{r}_1(X)$, and $\hat{v}_0(X)$, $\hat{v}_1(X)$, are amplitude components of disturbances of the jet radius and axial velocity, respectively. Since this study is concerned with a spatial instability analysis, ω is the real-valued frequency, and $\alpha = \alpha_r + i\alpha_i$ is complex-valued, whose real and imaginary parts represent the wavenumber and the growth rate in the axial direction, respectively. As Eqs. (9) show, perturbed state variables are decomposed into a slowly varying spatial amplitude function and a fast varying complex phase function. Linearized expansion of Eq. (1) using Eqs. (4) and (9) yields the following set of perturbation equations:

$$\begin{bmatrix} A & B \\ C & D \end{bmatrix} \begin{Bmatrix} \hat{r}_0 & \hat{r}_1 \\ \hat{v}_0 & \hat{v}_1 \end{Bmatrix} = \begin{bmatrix} 0 & M \\ 0 & N \end{bmatrix}, \tag{10}$$

and the matrix components are defined in the Appendix. Nontrivial solutions of the two homogeneous equations of (10), yield the following local dispersion relation:

$$D(\omega, \alpha, X) = AD - BC = 0, \tag{11}$$

or in polynomial form,

$$\begin{aligned} &\left(\frac{i\bar{r}^2\mathrm{Ca}}{8\mathrm{We}}\right)\alpha^5 - \left(\frac{1}{8} - \frac{\bar{r}^3}{2\mathrm{We}} + \frac{i\bar{r}^4\omega\mathrm{Ca}}{8\mathrm{We}}\right)\alpha^4 + \left(\frac{\bar{r}^2\omega}{4} + \frac{3i\mathrm{Ca}}{\mathrm{We}}\right)\alpha^3 - \\ &\left(\frac{1}{\bar{r}^2} + \frac{\bar{r}^4\omega^2}{8} + \frac{\bar{r}}{2\mathrm{We}} + \frac{3i\bar{r}^2\omega\mathrm{Ca}}{\mathrm{We}}\right)\alpha^2 + \left(2\omega + \frac{i\bar{r}^2\mathrm{Bo}}{\mathrm{We}}\right)\alpha - (\bar{r}^2\omega^2) = 0. \end{aligned} \tag{12}$$

The amplitude of the perturbations is found by solving the non-homogeneous equations in (10). After simplification, the following ordinary differential equation is obtained,

$$P(X)\frac{d\hat{r}_0(X)}{dX} + Q(X)\hat{r}_0(X) = 0, \tag{13}$$

where $P(X)$ and $Q(X)$ are defined in the Appendix. The solution of this ordinary differential equation can be written as

$$\hat{r}_0(X) = \hat{r}_0(0)\exp\left(-\int_0^X \frac{Q(X)}{P(X)}dX\right), \tag{14}$$

where $\hat{r}_0(0)$ is the initial jet radius perturbation that is in the following assigned to be one percent of the initial jet mean-radius. It is noted that $\hat{r}_1(X)$ and $\hat{v}_1(X)$ in Eqs. (9) do not appear in the final solution and are introduced for the purpose of obtained additional constraints to solve Eq. (10).

IV. RESULTS

In the following, the multiscale formulation that was developed in the previous section is used to investigate effects of surface tension, gravity, and viscosity on the growth-rate and perturbation dynamics of liquid jets. In this investigation we consider a range of representative operating conditions with Bond numbers of 0.01, 0.1, and 1, Weber numbers of 5 and 50, and Reynolds number of 1000. Relating these parameters to physical properties, they are representative for a water jet exiting from a nozzle with diameter ranging between 0.5 – 5 mm. In this context it is noted that, without further modifications, the model is also applicable to a wider range of conditions, including fountains and rising jets.

A. Model verification

For the case of zero Bond number, dispersion curves as function of frequency for three different Capillary numbers are presented in Fig. 3. The maximum growth rate and the corresponding wavenumber characterize the fastest growing (or the most probable) waves on the liquid surface that are eventually responsible for the breakup. From this figure, it can be seen that viscosity dampens the growth rate and shifts the maximum growth toward lower frequencies, resulting in the formation of larger droplets. The results obtained from the present multiscale formulation are compared with classical results by Leib & Goldstein [5], which are shown by symbols in Fig. 3. The excellent agreement serves as verification of the developed stability formulation based on Cosserat's equations.

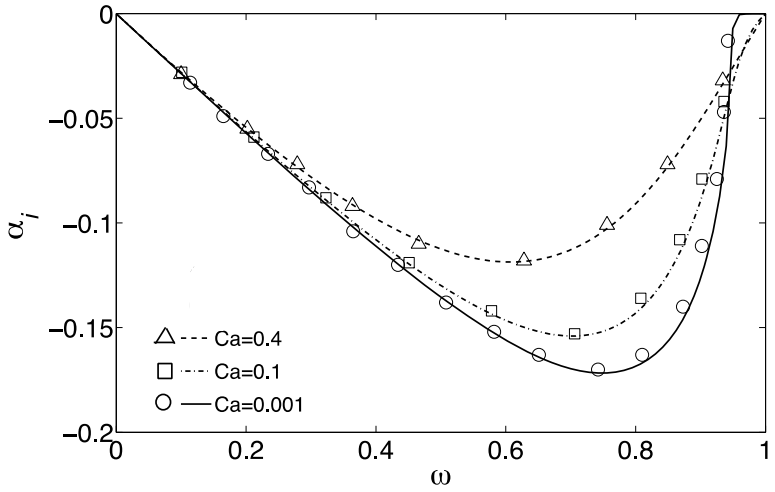

FIG. 3. Comparison of the growth rate obtained from the present model (lines) and classical results by Leib & Goldstein [5] (symbols) for *We*=5, *Bo*=0.

B. Critical Weber number

The critical Weber number, below which a liquid jet (without gravity effects) is absolutely unstable, and above which the jet is convectively unstable, was found by Leib & Goldstein [4] using the criteria of Briggs [20]. Figure 2 shows that for small Bond numbers, a local mean-flow assumption is valid. By considering this condition, we evaluate the critical Weber number from the dispersion relation as function of capillary number and different Bond numbers. Results of this analysis are illustrated in Fig. 4, showing that the critical Weber number decreases with increasing Bond numbers. Form these results, it can also be seen that in the limit of $\mathrm{Bo} \to 0$, the critical Weber number approaches the asymptotic value of Rayleigh-Chandrasekhar calculated by Leib and Goldstein [5]. In addition, current results show that in the limit of $\mathrm{Ca} \to 0$ the critical Weber number resulting a value of 3.10 which is very close to π based on Leib and Goldstein analysis [4].

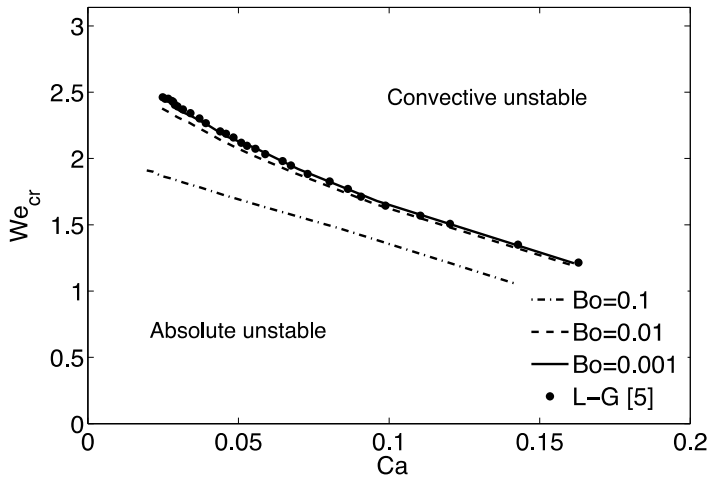

FIG. 4. Critical Weber number versus Capillary number for various Bond numbers.

Surface tension is the source of instabilities in low-speed jets. If the capillary force is sufficiently large compared to inertial forces, disturbances propagate both upstream and downstream, whereas in the opposite event, the inertia is dominant over the surface tension force and the disturbances can only propagate in the downstream direction. In a downward-pointing jet, gravity enhances the inertia. Therefore, disturbances are not able to propagate upstream except for very low Weber numbers. Dripping is a candidate for the manifestation of an absolute instability and the transition between absolute and convective instability is comparable with the transition from dripping to jetting [21]. In fact, part of the disturbances will propagate back to the nozzle tip to prevent the formation of a jet of any length. Results in Fig. 4 are in agreement with those of Clanet & Lasheras [22] and Ambravaneswaran et al. [6] and show that by increasing the Bond number, the transition from dripping to jetting occurs at lower Weber numbers.

C. Effects of gravity

Mean jet profiles that were obtained from the numerical solution of Eqs. (5) for different *We* and *Bo* numbers are plotted in Fig. 5. As shown in this figure, at low Weber numbers, the effect of

Bond number on the jet contraction is considerable. However, with increasing Weber number, the effect of gravity on the jet profile reduces. In addition, results show that the maximum jet slope occurs at the nozzle exit and further down the jet, the liquid jet converges to a near-parallel profile.

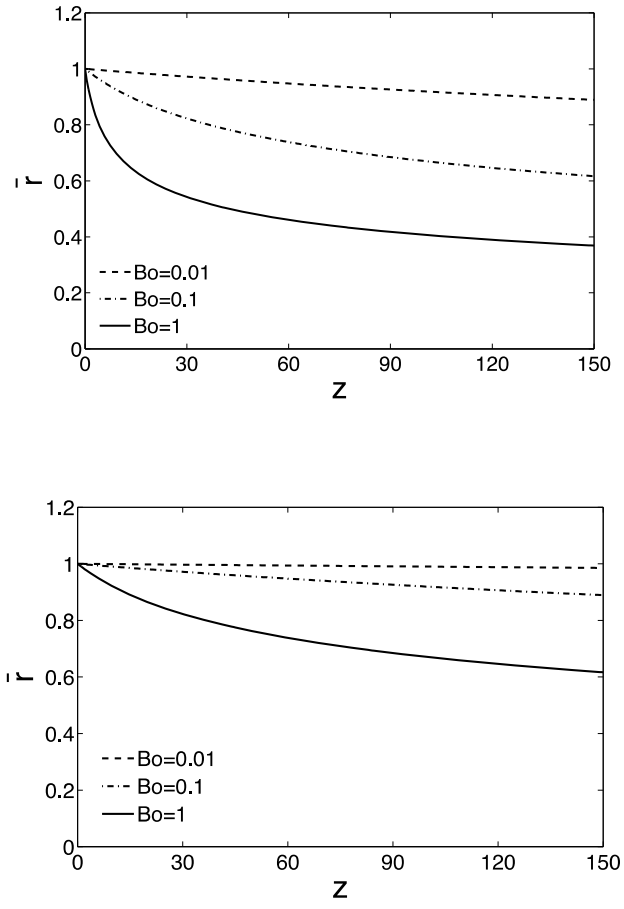

FIG. 5. Variation of unperturbed jet radius (base flow) with axial distance for various Bond numbers (top: Ca=0.005, We=5, bottom: Ca=0.05, We=50).

Results from the stability analysis are summarized in Figs. 6 and 7 for the selected cases of We = 5 and 50, respectively. From left to right, results for increasing Bond number are shown (Bo={0.01, 0.1, 1}). The first row shows the growth rate α_i as function of axial distance and

perturbation frequency, the second row shows the corresponding wavenumber α_r, and the third row illustrates the perturbation amplitude, which is evaluated as:

$$\bar{r} - |\hat{r}_0| \exp\left(-\frac{1}{\varepsilon} \int_0^X \alpha_i \, dX \right). \tag{15}$$

For reference, the blanked-out area indicates the break-up region for which relation (15) becomes less than zero. It is noted that this criterion provides only a qualitative indication for the reason that the break-up point is affected by the initial perturbation magnitude (which is here set to a numerical value of 1% of the mean-jet radius) and nonlinear processes, which are not considered in this analysis. Finally, the last row illustrates the mean (dashed) and instantaneous (solid line) liquid jet radii at the most unstable forcing frequency.

From these results it can be seen that by increasing the Weber number, the instability growth rate decreases, which is in agreement with the well-known breakup curves as described by Lin & Reitz [21]. Importantly, the results also show that by increasing the Bond number the instability grows faster. In addition, the range of unstable wavenumbers increases and the peak of the curve shifts towards higher frequencies. These results are in agreement with experiments [23, 24], showing that the breakup length is reduced under consideration of gravity, resulting in the formation of smaller droplets. The perturbed jet profile is also plotted in Figs. 6 and 7 for a range of *We* and *Bo* numbers. The fluctuating jet radius is obtained as solution to Eq. (14), assuming an initial amplitude of $\hat{r}_0(0) = 0.01$. Results confirm that for low Weber numbers and high Bond numbers, the mean flow is considerably contracting and a nonparallel analysis is required to perform the stability analysis.

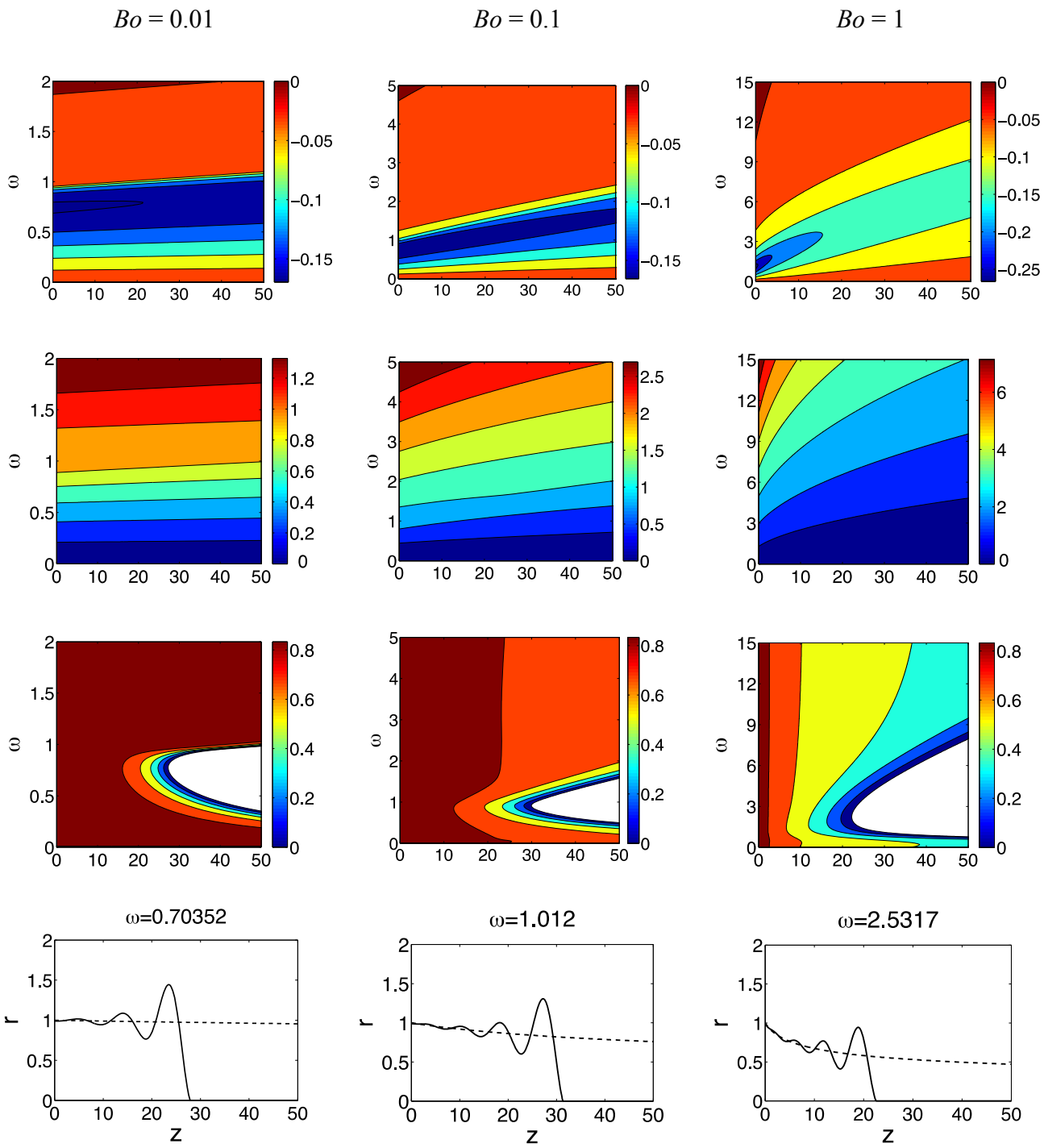

FIG. 6. (Color online) Results from multiscale analysis for different Bond numbers with $Ca = 0.005$ and $We = 5$, showing (1st row) growth rate, (2nd row) wavenumber, (3rd row) jet magnitude, and (4th row) mean and instantaneous jet radius for most unstable perturbation frequency (dashed line: base flow, solid line: perturbed flow).

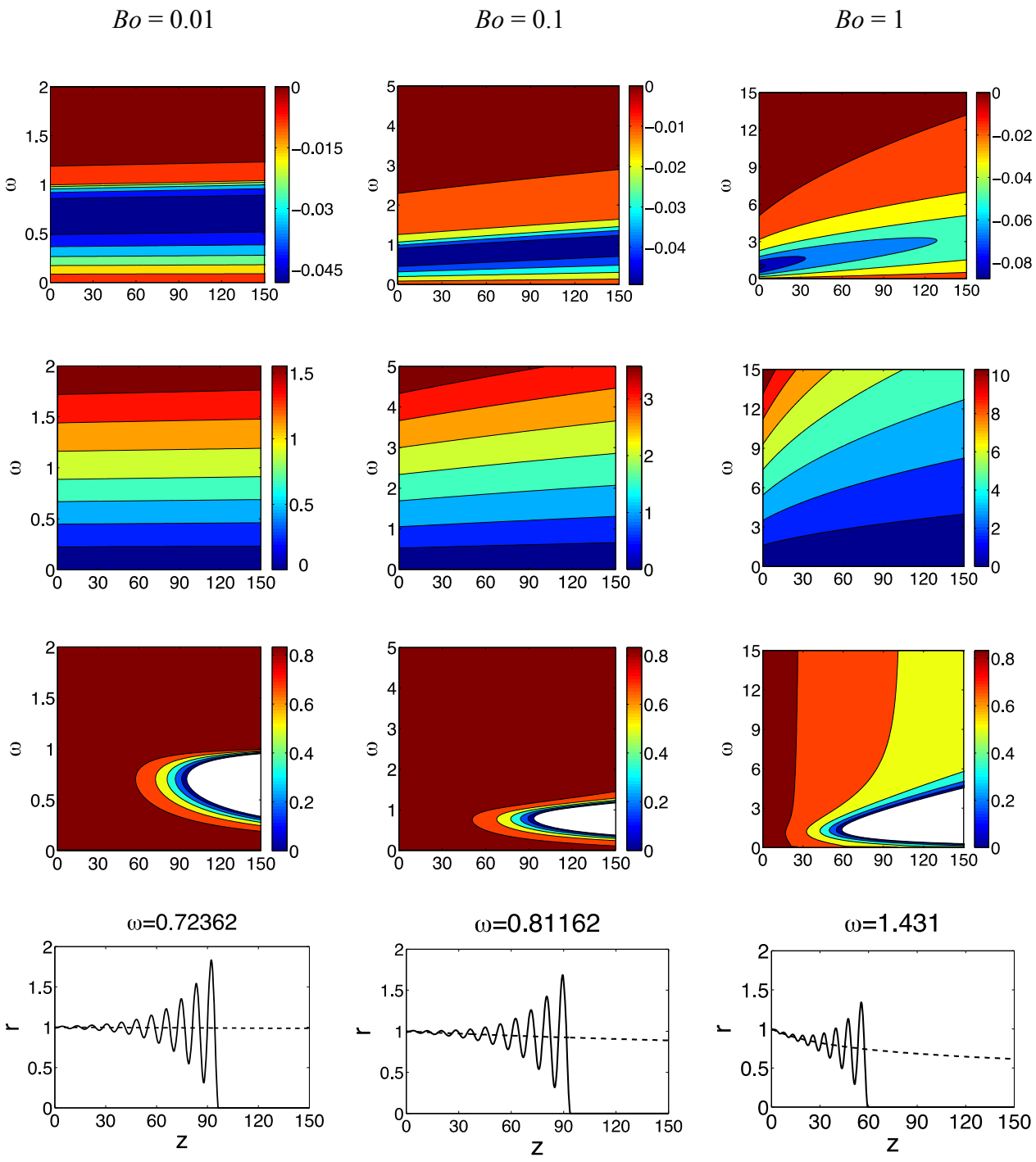

FIG. 7. (Color online) Results from multiscale analysis for different Bond numbers with $Ca = 0.05$ and $We = 50$, showing (1st row) growth rate, (2nd row) wavenumber, (3rd row) jet magnitude, and (4th row) mean and instantaneous jet radius for most unstable perturbation frequency (dashed line: base flow, solid line: perturbed flow).

As a result of the assumption that the perturbation magnitude remains small relative to the jet radius, linear analysis fails near the point of jet breakup. Therefore, linear methods do not provide an adequate description of the droplet size. Despite this shortcoming, the linear stability analysis provides a qualitative description of the physical mechanisms involved in the various regimes of the jet breakup process and this mechanism remains the same during the nonlinear evolution [17]. The liquid jet breaks up at a streamwise location at which the magnitude of the fluctuating part becomes equal to the mean jet radius (see Eq. (15)). The effect of gravity on the jet breakup length can be seen in Figs. 6 and 7. The results show that by increasing the Bond number, the breakup length decreases, providing a theoretical explanation for the experimentally observed behavior by Howes and coworkers [23, 24].

V. CONCLUSIONS

A multiscale analysis was performed to examine the onset and growth of capillary instabilities in liquid jets under consideration of effects of surface tension, viscosity, and gravitational forcing. A theoretical formulation was developed using Cosserat's equations, and dispersion relations and expressions for the spatio-temporal evolution of the perturbation amplitude were derived. To confirm the validity of this approach, comparisons with classical linear stability results for the special case of zero Bond-number were presented, and excellent agreement is obtained. From the solution of the dispersion relation it was shown that the critical Weber number decreases with increasing Bond number, which explains the reason for shifting the transition between dripping and jetting to lower Weber numbers in the case of considering gravity effects.

Following this characterization, the analysis was extended to investigate the instability dynamics over a range of relevant operating conditions that are represented in terms of Bond,

Weber, and Capillary numbers. The results presented in this work reveal that by increasing gravitational forcing, the jet instability increases, the maximum growth rate shifts toward shorter waves, and the cut-off frequency increases.

Apart from the physical insight that is obtained from this analysis, results of this study could also be of value as canonical test cases for the algorithmic assessment and the verification of high-fidelity multiphase simulation codes [25]. Although only the linear regime is considered, the accurate numerical prediction of phase-speed and perturbation growth-rate represents considerable challenges to numerical methods that can be systematically addressed through direct comparisons against theoretical results from the present multiscale analysis. The herein presented stability results provide access to different instability behaviors (characterized by growth rate, forcing frequency, wavelength, and breakup point), so that the complexity of the test cases can be adjusted.

ACKNOWLEDGMENTS

The authors gratefully acknowledge financial support through the NSF CAREER program with Award No. CBET-0844587.

APPENDIX

$$A = -i\omega + i\bar{v}\alpha \tag{A1}$$

$$B = \frac{i\bar{r}\alpha}{2} \tag{A2}$$

$$C = -\frac{1}{\mathrm{We}}\left(i\alpha - i\bar{r}^2\alpha^3\right) - \frac{2\mathrm{Bo}}{\mathrm{We}}\bar{r} \tag{A3}$$

$$D = -i\bar{r}^2\omega + i\alpha + -\frac{i}{8}\bar{r}^4\alpha^2\omega + \frac{1}{8}i\bar{r}^2\alpha^3 + \frac{\mathrm{Ca}}{\mathrm{We}}\left(\frac{1}{8}\bar{r}^4\alpha^4 + 3\bar{r}^2\alpha^2\right) \tag{A4}$$

$$M = M_1\hat{r}_0 + M_2\hat{r}_{0X} + M_3\hat{v}_0 + M_4\hat{v}_{0X} \tag{A5}$$

$$N = N_1\hat{r}_0 + N_2\hat{r}_{0X} + N_3\hat{v}_0 + N_4\hat{v}_{0X} \tag{A6}$$

$$M_1 = -\frac{\bar{v}_X}{2} \tag{A7}$$

$$M_2 = -\bar{v} \tag{A8}$$

$$M_3 = -\bar{r}_X \tag{A9}$$

$$M_4 = -\frac{\bar{r}}{2} \tag{A10}$$

$$N_1 = -2\bar{r}\bar{v}\bar{v}_X - \frac{1}{\mathrm{We}}\left(\bar{r}\bar{r}_X\alpha^2 + 3\bar{r}^2\alpha\alpha_X\right) + \frac{6\mathrm{Ca}}{\mathrm{We}}\left(i\bar{r}\bar{v}_X\alpha\right) \tag{A11}$$

$$N_2 = \frac{1}{We}\left(1 - 3\bar{r}^2\alpha\right)^2 \tag{A12}$$

$$\begin{aligned} N_3 = {} & -\bar{r}^2\bar{v}_X + \frac{1}{2}\bar{r}^3\bar{r}_X\omega\alpha - \frac{1}{2}\bar{r}\bar{r}_X\alpha^2 + \frac{1}{8}\bar{r}^4\omega\alpha_X - \frac{3}{8}\bar{r}^2\alpha\alpha_X \\ & + \frac{i\mathrm{Ca}}{\mathrm{We}}\left(\bar{r}^3\bar{r}_X\alpha^3 + \frac{3}{4}\bar{r}^4\alpha\alpha_X + 6\bar{r}\bar{r}_X\alpha + 3\bar{r}^2\alpha_X\right) \end{aligned} \tag{A13}$$

$$N_4 = -1 + \frac{1}{4}\bar{r}^4\alpha\omega - \frac{3}{8}\bar{r}^2\alpha^2 + \frac{i\mathrm{Ca}}{\mathrm{We}}\left(\frac{1}{2}\bar{r}^4\alpha^3 + 6\bar{r}^2\alpha\right) \tag{A14}$$

$$P = \left(N_2 - \frac{C}{A}M_2\right) - \left(N_4 - \frac{C}{A}M_4\right)\frac{A}{B} \tag{A15}$$

$$Q=\left(N_1-\frac{C}{A}M_1\right)-\left(N_3-\frac{C}{A}M_3\right)\frac{A}{B}-\left(N_4-\frac{C}{A}M_4\right)\left(\frac{A_X B-AB_X}{B^2}\right) \quad \text{(A16)}$$

---

[1] J. Eggers and E. Villermaux, Rep. Prog. Phys., **71**, 036601, 79 (2208).

[2] Rayleigh, Proc. R. Soc., **29**, 71 (1879).

[3] J. B. Keller, S. I. Rubinow, and Y. O. Tu, Phys. Fluids, **16**, 2052 (1973).

[4] S. J. Leib and M. E. Goldstein, J. Fluid Mech., **168**, 479 (1986).

[5] S. J. Leib and M. E. Goldstein, Phys. Fluids, **29**, 952 (1986).

[6] B. Ambravaneswaran, H. J. Subramani, S. D. Phillips, and O. A. Basaran, Phys Rev Lett., **93**, 034501, 4 (2004).

[7] J. M. Montanero, M. A. Herrada, C. Ferrera, E. J. Vega, and A. M. Ganan-Calvo, Phys. Fluids, **23**, 122103, 12 (2011).

[8] A. E. Green, Int. J. Eng. Sci., **14**, 49 (1976).

[9] F. J. Garcia and A. Castellanos, Phys. Fluids, **6**, 2676 (1994).

[10] J. Eggers, Rev. Mod. Phys., **69**, 865 (1997).

[11] D. B. Bogy, Phys. Fluids, **21**, 190 (1978).

[12] D. B. Bogy, J. Appl. Mech., **45**, 469 (1978).

[13] D. B. Bogy, IBM J. Res. Dev., **23**, 87 (1979).

[14] D. B. Bogy, Phys. Fluids, **22**, 224 (1979).

[15] G. Amini and A. Dolatabadi, Phys. Fluids, **23**, 8, 084109, (2011).

[16] G. Amini and A. Dolatabadi, Int. J. Multip. Flow, **42**, 96 (2012).

[17] D. B. Bogy, Ann. Rev. Fluid. Mech., **11**, 207 (1979).

[18] P. Huerre and M. Rossi, "Hydrodynamics and nonlinear instabilities" Ed. by C. Godreche and P. Manneville, Camb. Univ. Press, Chap. 2 (1998).

[19] D.G, Crighton and M. Gaster, J. Fluid Mech. **77**, 397 (1976).

[20] R.J. Briggs, "Electron-Stream Interaction with Plasmas" MIT Press, Cambridge, MA, (1964).

[21] S. P. Lin and R. D. Reitz, Ann. Rev. Fluid Mech., **30**, 85 (1998).

[22] C. Clanet and J.C. Lasheras, J. Fluid Mech. **383**, 307 (1999).

[23] B.S. Cheong and T. Howes, Chem. Eng. Sci., **59**, 2145 (2004)

[24] A.P.R. Edwards, B.P. Osborne, J.M. Stoltzfus, T. Howes, and T.A. Steinberg, Phys. Fluids, 14, 3432 (2002).

[25] A. Prospretti (Ed), "Computational methods for multiphase flow", Camb. Univ. Press, (2009).